SCIENTIFIC REPORTS

OPEN

Many-body Tunneling and Nonequilibrium Dynamics of Doublons in Strongly Correlated Quantum Dots

WenJie Hou[1], YuanDong Wang[1], JianHua Wei[1], ZhenGang Zhu[2] & YiJing Yan[3]

Quantum tunneling dominates coherent transport at low temperatures in many systems of great interest. In this work we report a many–body tunneling (MBT), by nonperturbatively solving the Anderson multi-impurity model, and identify it a fundamental tunneling process on top of the well–acknowledged sequential tunneling and cotunneling. We show that the MBT involves the dynamics of doublons in strongly correlated systems. Proportional to the numbers of dynamical doublons, the MBT can dominate the off–resonant transport in the strongly correlated regime. A $T^{3/2}$–dependence of the MBT current on temperature is uncovered and can be identified as a fingerprint of the MBT in experiments. We also prove that the MBT can support the coherent long–range tunneling of doublons, which is well consistent with recent experiments on ultracold atoms. As a fundamental physical process, the MBT is expected to play important roles in general quantum systems.

Quantum tunneling is ubiquitous in quantum systems[1–7]. Two basic tunneling processes have been investigated: the first–order sequential tunneling (ST) and the second–order cotunneling (CT)[8–10]. Theoretically, both ST and CT can be well described by a single–particle picture. On the other hand, quantum tunneling deeply involved many–body interactions (shortened with many–body tunneling (MBT)) inevitably exists and dominates in many strongly correlated systems. The MBT is defined as the electron tunneling through the singly to doubly occupation transition, which includes all high–order tunneling processes beyond the second order. Until now, our understanding of the MBT has been severely hindered by the difficult nonperturbative treatment of the many-body dynamics. In the present work, we deal with this issue and uncover that the MBT involves coherent production and decay of doublons with nonperturbative and nonequilibrium characters.

Doublon was initially proposed for the state of doubly-occupied site in Hubbard model[11], an excitation with respect to the half-filled Mott-insulator ground state. In strongly correlated systems, the doublon-holon (unoccupied sites) binding plays important role[12], which was proved to be closely related to the Mott transition and high-temperature superconductivity[13]. Recently, the Hubbard models have been successfully simulated in ultracold atoms. In 2006, doublons with long lifetimes were observed in ultracold ^{87}Rb atoms[14]. Since then, there have been extensive studies on the properties of doublons in Bose- and Fermi-Hubbard models in ultracold atoms[15–22]. Among those, the dynamics of doublons is of special interest, which can facilitate the understanding of the far-from-equilibrium dynamics of strongly correlated systems. The experiments of Fermi-Hubbard model (ultracold ^{40}K atoms) found the decay rate of doublon scaling as $\tau^{-1} \propto \exp(-U/t)$, where U is the on-site electron-electron ($e-e$) interaction and t is the tunneling coupling between nearest-neighbor sites[16]. Similar relation was theoretically verified in Bose-Hubbard model[18]. The exponential dependence clearly originates from the many-body character of the dynamics of doublons, which is far beyond the single-particle picture in the strongly correlated regime ($U/t \gg 1$).

[1]Department of Physics, Renmin University of China, Beijing, 100872, China. [2]School of Electronic, Electrical and Communication Engineering, University of Chinese Academy of Sciences, Beijing, 100049, China. [3]Hefei National Laboratory for Physical Sciences at the Microscale and iChEM (Collaborative Innovation Center of Chemistry for Energy Materials), University of Science and Technology of China, Hefei, Anhui, 230026, China. Correspondence and requests for materials should be addressed to J.W. (email: wjh@ruc.edu.cn) or Z.Z. (email: zgzhu@ucas.ac.cn) or Y.Y. (email: yanyj@ustc.edu.cn)
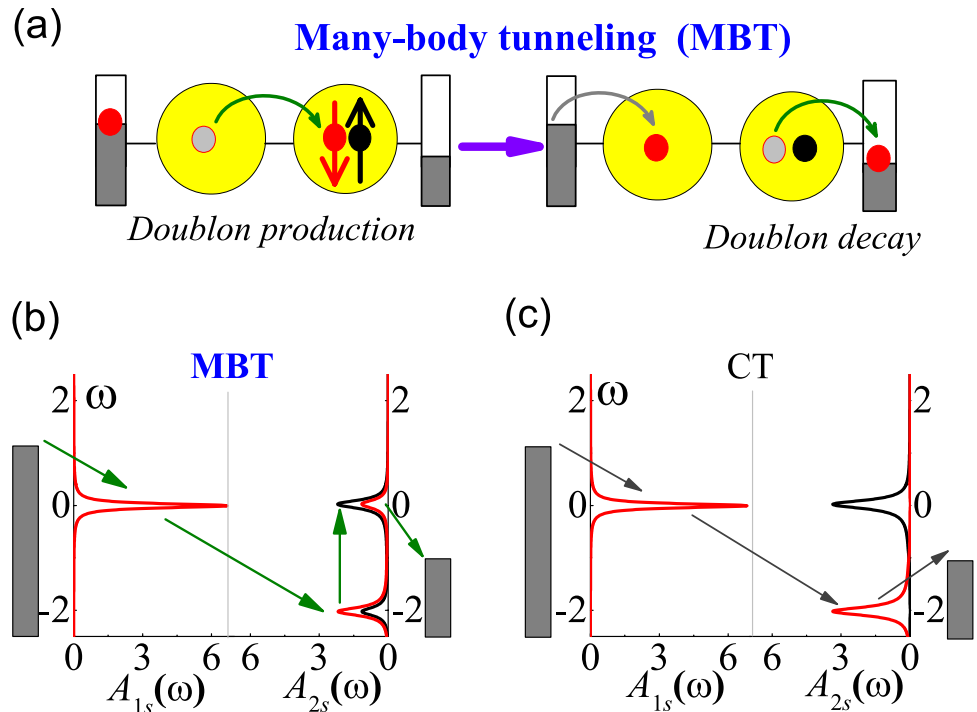
Figure 1. (**a**) Schematic diagram of the many–body tunneling (MBT) in DQDs. (**b**) and (**c**) show calculated nonequilibrium spectral functions $A_{1s}(\omega)$ and $A_{2s}(\omega)$ with $s = \downarrow$ (red) and $s = \uparrow$ (black), and illustrated processes of the MBT and CT respectively. The accurate HEOM is performed in (**b**) and the HEOM truncated at tier level $L = 1$ in (**c**) at $t = 0.01$ meV, and $eV = U = 2.0$ meV. $\epsilon_{2\downarrow} = \epsilon_{2\uparrow} = -2.0$ meV. Due to the lifted spin degeneracy of QD1, $A_{1\downarrow(\uparrow)}$ peaks at $\epsilon_{1\downarrow} = 0$ meV ($\epsilon_{1\uparrow} = 3.0$ meV (not shown)). The dot-reservoir coupling strength and temperature are $\Gamma = 0.1$ meV and $T = 0.1$ meV, respectively.

Although the doublon have been studied in ultracold atom systems, the connection to the MBT and its many-body nature are not fully appreciated. We demonstrate that the doublon dynamics can be described by two-particle density matrix and is a kind of MBT naturally originating from strong Coulomb interaction. We select multi-impurity Anderson models[23] for illustration due to the tunable system parameters, e.g. double, triple and quadruple quantum dots (DQDs, TQDs and QQDs) connected to two biased reservoirs. The models are nonperturbatively solved by the hierarchical equations of motion approach (HEOM). The intrinsic features of the MBT and doublon are studied and their universality is addressed.

MBT in DQDs

Fundamentally, both ST and CT are only related to the reduced time–dependent single–particle density matrix, $\rho(t)$, thus their current is not sensitive to U. By contrast, the MBT engages reduced two–particle density matrix, $\pi(t)$. There are altogether three kinds of $\pi(t)$, corresponding to three kinds of basic physical processes (see the equations of the HEOM in Ref. Jin08234703). They are: 1) the Kondo effect, described by $\pi_k(t) = \text{tr}\left[b_{j'\bar{s}}^{+}c_{i\bar{s}}c_{is}^{+}a_{js}\rho(t)\right]$ and its Hermitian conjugation; 2) the MBT, described by $\pi_m(t) = \text{tr}\left[n_{i\bar{s}}c_{is}^{+}a_{js}\rho(t)\right]$ (doublon production, see Fig. 1 (a)) and its Hermitian conjugation (doublon decay); and 3) the tunneling of doublon–holon excitation, described by $\pi_d(t) = \text{tr}\left[c_{i\bar{s}}^{+}c_{is}b_{j'\bar{s}}^{+}a_{js}\rho(t)\right]$ (doublon) and its Hermitian conjugation (holon). In these expressions, c_{is} (c_{is}^{+}), with $s = \uparrow, \downarrow$, denotes the annihilation (creation) operator matrix of an electron in the specified spin state in the i th dot; $n_{i\bar{s}} = c_{i\bar{s}}^{+}c_{\bar{s}}$ is the number operator with opposite spin of s; a_{js} and b_{js} denote dot or bath operator matrixes which can be the same or different. In the present work, neither the Kondo effect nor the doublon–holon excitation plays a role within the investigated parameter range, thus we precisely work out the MBT current.

Although it is accompanied by the production and decay of doublons, based on the analytical analysis, it is noted that the MBT only concerns the tunneling of electrons, rather than the direct tunneling of doublon–holon excitations. The latter is another important many–body effect which will be addressed in future works. We also comment that all of the physical quantities obtained from HEOM calculations, including current, occupation number and spectral functions, will be self–consistently checked to achieve their precise values in what follows. Our numerical results prove that no other contributions to the current besides ST, CT and MBT, which confirms that the MBT involves all high–order tunneling processes beyond the second order.

By referring Fig. 1(a), one can deduce that the Kondo spin screening may occur if spin flips during the doublon decay[24, 25]. In single QD, the Kondo resonance dominates the transport in the impurity magnetic moment regime, overwhelming the MBT by competition. However, the MBT may make leading contribution in multi-QD systems. First of all, we introduce Pauli spin blockade (PSB) in DQDs. The PSB results from the Pauli's exclusion principle which prevents the spin triplet from transporting out of the DQDs, and is characterized by the electron
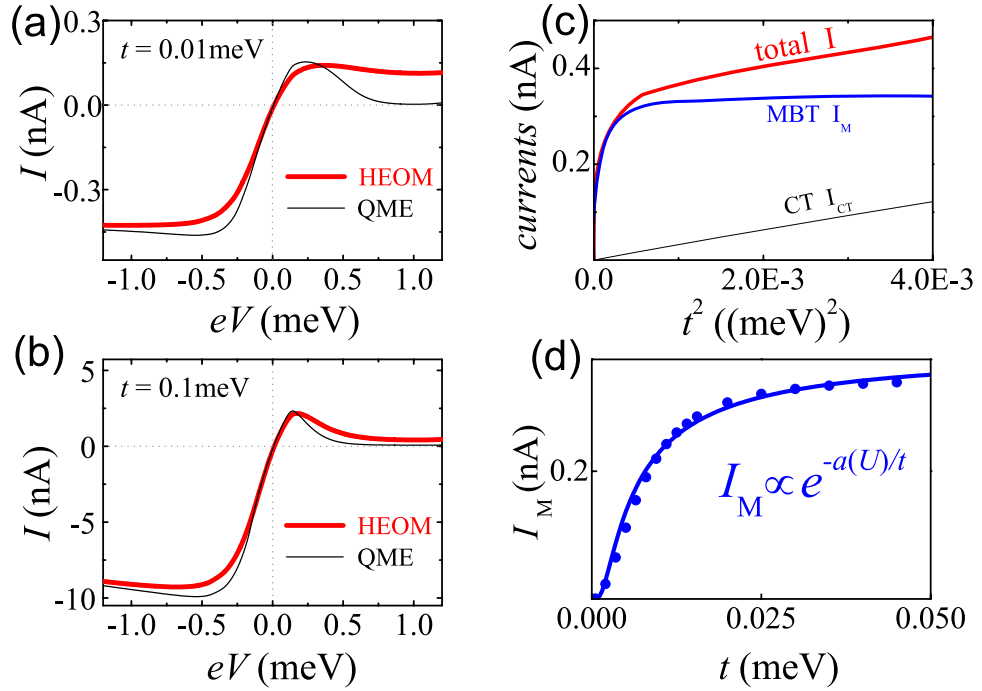
Figure 2. The I–V curves are calculated at $t = 0.01$ meV in (**a**), and $t = 0.1$ meV in (**b**), for the DQDs, and $U = 2.0$ meV fixed. (**c**) The I, I_M, and I_{CT} and varying with t^2 are shown at $eV = U$. (**d**) The dependence of I_M on t is given. The dots are numerical data and the solid line is the plot of the function $I_M \propto \exp[-\alpha(U)/t]$ with $\alpha(U)$ being a U-dependent parameter.

density accumulation as well as the current suppression in one bias direction[26–28]. The reason of choosing the PSB regime is that the MBT dominates the transport leading to a finite current even when the CT is blocked. In fact, the current can be large enough to degrade the PSB effect, which can be a measurable symbol of the MBT (Fig. 2(a)).

To make the discussion concrete, we numerically calculate the nonequilibrium spectral functions $A_{is}(\omega)$ in the PSB regime, as shown in Fig. 1(b) and (c). The MBT involves four events occurring almost simultaneously. i) A $\downarrow$-spin electron tunnels from the left reservoir to QD1; ii) The excess $\downarrow$-spin tunnels from the QD1 to QD2; iii) The $\downarrow$-spin electron in the QD2 excites to the doubly occupied level (doublon production); and iv) The doubly occupied $\downarrow$-spin electron in the QD2 tunnels to the right reservoir (doublon decay). A key point is that the MBT strongly depends on U in both doublon production and decay processes. In comparison, the CT shown in Fig. 1c) can be well described by the second-order time-nonlocal quantum master equation (QME)[29]. Different to the MBT, the tunneling from the QD1 to the right reservoir is now via the singly occupied level of the QD2, without doublon production nor decay process. This leads to insensitivity of the CT to U, which is an essential difference of the CT to the MBT.

The Anderson multi–impurity model is adopted for N–QD ($N = 2, 3$ or 4) systems. The total Hamiltonian reads $H_{total} = H_{sys} + H_{res} + H_{sys-res}$. The Hamiltonians of reservoirs are $H_{res} = \sum_{\alpha ks}(\epsilon_{\alpha ks} + \mu_\alpha)\hat{c}^\dagger_{\alpha ks}\hat{c}_{\alpha ks}$, $\alpha = L, R$, under the bias $V = (\mu_L - \mu_R)/e$, where $\hat{c}_{\alpha ks}$ ($\hat{c}^\dagger_{\alpha ks}$) denotes the annihilation (creation) operator of an electron in the specified spin state in the α-reservoir with wave vector k. We set $E_F = \mu_L^{eq} = \mu_R^{eq} = 0$ at equilibrium and $\mu_L/e = -\mu_R/e = V/2$. The system-reservoir coupling is $H_{sys-res} = \sum t_{\alpha kis}\hat{c}^\dagger_{is}\hat{c}_{\alpha ks} +$ h.c. The hybridization function is assumed to be a Lorentzian form $J_{\alpha is}(\omega) = \pi\sum_k t_{\alpha kis}t^*_{\alpha kis}\delta(\omega - \epsilon_{\alpha ks}) = \frac{\Gamma W^2}{\omega^2 + W^2}$, with $W = 4$ meV fixed in this letter. The QD-reservoir coupling strength Γ will be specified below. The Hamiltonian for central N-QD is

$$H_{sys} = \sum_{i=1,s}^{N} \epsilon_{is}\hat{n}_{is} + U\sum_i \hat{n}_{i\uparrow}\hat{n}_{i\downarrow} + t\sum_{<ij>,s}(\hat{c}^\dagger_{is}\hat{c}_{js} + \text{h.c.}).$$

For DQD case, we lift the spin degeneracy of the QD1. This can be achieved with a local spin–splitting micro-magnet[30], resulting in $\mu_R < \epsilon_{1\downarrow} < \mu_L < \epsilon_{1\uparrow}$ for QD1. The spin degeneracy of the QD1 will be restored later. The spin degeneracy of the QD2 remains, with $\epsilon_{2\uparrow} = \epsilon_{2\downarrow}$ and $\epsilon_{2s} < \mu_R < \epsilon_{2s} + U < \mu_L$. The single–occupied levels, ϵ_{1s} and ϵ_{2s}, are tuned via appropriate local gate voltages to achieve the optimal PSB stability; i.e., $\epsilon_{1\downarrow} = \epsilon_{2s} + U = 0$ [26–28]. To study the long-range MBT in the TQD and QQD, a tilt energy E_i is added to each dot as in ultracold atom experiments[7], i.e., $H_{sys} = H_{sys} + \sum_{i,s}E_i\hat{n}_{is}$. For the tilted TQDs (see the insert of Fig. 5(a)), $E_1 = -E_3 = E$, $E_2 = 0$; and for the tilted QQDs (see the insert of Fig. 5(c)), $E_1 = -E_4 = 3E/2$, $E_2 = -E_3 = E/2$, where E is the nearest–neighbor tilt energy.

The multi-impurity Anderson model is solved using the HEOM approach[31, 32]. This approach supports accurate and efficient evaluations of various steady–state and transient properties[32–35] (for more details, please refer to Ref. [YeWIREs] and references therein). It has been demonstrated that the HEOM approach achieves the same level of accuracy as the latest high–level numerical renormalization group and quantum Monte Carlo approaches for the prediction of various dynamical properties at equilibrium and nonequilibrium[31].

The current–voltage characteristics at $t = 0.01$ and 0.01 meV are shown in Fig. 2(a) and (b), respectively. For comparison, the QME results essentially from the perturbative treatment are shown. Let us examine closely the forward current, $I(V > 0)$. In both $t = 0.01$ meV and $t = 0.01$ meV cases, the QME currents show negative differential conductances, due to the transition from the resonant to off–resonant tunneling[36, 37]. At large V, the QME currents tend to near-zero constant value resulting from the CT, with a ratio of $I_{peak}/I_{const} \approx 50$. For precise HEOM currents (including the nonperturbative MBT currents), things are different. In $t = 0.01$ meV case, the MBT current is increased and the negative differential conductance almost vanishes. Although in the $t = 0.1$ meV case, both the QME and HEOM currents display similar negative differential conductance, it should be pointed out that the HEOM current in Fig. 2(b) gives us $I_{peak}/I_{const} \approx 4$, *which matches the experimental data well*[36]. Although some other external mechanisms concerning the leakage current in the PSB regime have also been proposed in literatures[38], here we provide a more intrinsic and universal one.

Figure 2(c) depicts the total current I, and its two compositions, I_M (for the MBT) and I_{CT} (for the CT), as functions of t^2 at $U = 2.0$ meV. I is the converged HEOM result, with I_{CT} for the time-nonlocal QME, and $I_M = I - I_{CT}$. In contrast to $I_{CT} \propto t^2$ resulting from the second-order perturbation theory, I_M exhibits a strong nonlinearity before saturation. By fitting the numerical data of I_M in Fig. 2(d), we find $I_M \propto \exp[-\alpha(U)/t]$, where $\alpha(U)$ is a parameter approximately proportional to U. It means that the MBT current has a similar dependence on U/t to the decay rate of doublons observed in Ref. [Strohmaier10080401], which originates from the many-body character of the doublon dynamics. It is more important that these features are rather general, beyond the case of $eV = U$ in Fig. 2(c) and (d).

For spin-nondegenerate-QD1 case, the tunneling current is basically carried by down spins, i.e., $I \simeq I^\downarrow$, with $I^\uparrow \simeq 0$. As shown in Fig. 1, $I_M^\downarrow$ should be closely related to the number of doublons generated in QD2 and decayed into the right reservoir. We call this part of doublons as 'dynamical doublons' and denote their number as n_{DD}. In the DQDs, $n_{DD}(t) = 1/2 - n_{2\uparrow}(t)$, where $n_{2\uparrow}$ is the $\uparrow$-spin occupation number in QD2. For the uncoupled limit $n_{2\uparrow}(t = 0) = 1/2$ leading to $n_{DD}(t = 0) = 0$. $I_M^\downarrow$ is evaluated as a function of n_{DD} for different Γ and U in Fig. 3 (a) and (b), respectively. Remarkably, $I_M^\downarrow$ keeps a fundamental linear function of n_{DD}, i.e.

$$I_M^\downarrow = k n_{DD} = k\left(\frac{1}{2} - n_{2\uparrow}\right),$$

(1)

in all regimes of t, across a broad range of U, Γ, and temperature T. For the parameters chosen in Fig. 2(c), $k = 0.75$ nA. At $t > 0.05$ meV, $n_{2\uparrow} = 0.05$ and $n_{DD} = 0.45$, thus $I_M^\downarrow = 0.33$ nA, which is completely consistent with the saturation current shown in Fig. 2(c). $I_M \propto n_{DD}$ proves that the dynamical doublons are the only carriers of I_M, namely, the MBT precisely describes the dynamics of doublons, as we argued above.

The ideal linear plots in Fig. 3(c) shows further scaling laws of the slope k on the ratio of Γ/U, $k \propto (\Gamma/U)^2$. In Fig. 3(d), we prove the temperature dependence of the MBT current as, $I_M(=I_M^\downarrow) \propto T^{3/2}$, which is distinctly different from the T^2-dependence of I_{CT}[9]. This unconventional T dependence, originally attributed to the intrinsic many-body character of the MBT, can be conveniently verified by experiments.

It is necessary to extend the study to the spin-degenerate case in which the local Zeeman splitting in QD1 is removed. We thus choose $\epsilon_{1\downarrow} = \epsilon_{1\uparrow} = 0$ and keep other parameters unchanged. The corresponding I–V curves are shown in Fig. 4(a), the counterparts to Fig. 2(a). It is observed that the MBT current still dominates in the weak coupling regime at high bias. Apparently, the main features of the MBT current in the spin-degenerate case are basically the same as those of the spin–nondegenerate case. Figure 4(b) is the spin–degenerate counterpart to Fig. 2(c). Again the basic features remain unaltered. In particular, I_M also increases exponentially with t^2, and then gradually saturates at a constant value. From the above results, we can conclude that the MBT characters still hold well in the spin–degenerate case. In other words, the MBT is a general process.

Long-range MBT

Now, we are on the position to demonstrate the coherent long-range MBT in larger systems than DQDs. In recent experiments of the Bose-Hubbard chain at $t \ll U$, long-range tunneling over up to five sites were observed as resonances in the number of doublons when the nearest-neighbour tilt energy (E) is tuned to integer fractions of U[7]. Let us prove that the observations arise from the long-range MBT by numerical results in tilted TQDs and QQDs (see inserts in Fig. 5(a) and (c)). Figure 5(a) depicts the dependence of I, I_M and I_{CT} on t^4 at $eV = 1.5$ meV for the spin degenerate TQD with $E = U/2$. Not surprisingly, all of them behave in a similar manner as those in DQD. Since the number of tunneling barriers doubles now, we have $I_{CT} \propto t^4$.

In tilted QDs, I_{CT} can not be blocked as that in the PSB region, thus it is mixed with I_M in observed I. In order to separate out the direct contribution of the MBT, we define $\gamma \equiv (I_M/I \times 100\%)$. Figure 5(b) shows the dependence of γ on the ratio of E/U for the TQDs. The case of titled DQDs is shown in the insert for the purpose of comparison. For the TQDs, a resonant peak at $E = U/2$ is clearly seen; while for the DQDs, that peak shifts to $E = U$, with the peak position unchanged at different t. The maximum value of γ up to 75% in TQDs further proves that the resonance at $E = U/2$ results from the long-range MBT rather than the CT which in fact has been excluded already by the strong U-dependence of the resonance. Both the peak structure and the peak position for the DQDs and TQDs shown in Fig. 5(b) are well consistent with experimental observations for Cs atoms in optical lattice in Ref. [Meinert141259], which suggests that our theory shares the same physics of long-range tunneling of doublons in experiments about ultracold atoms although their objects of study are quite different.
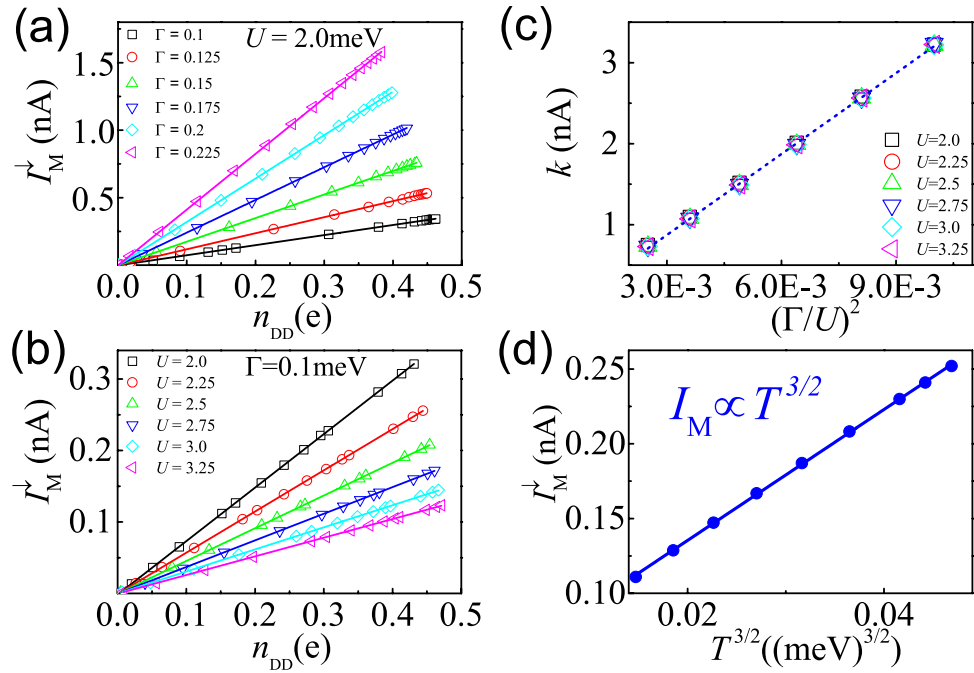
Figure 3. The curves of $I_M^{\downarrow}$ as a function of the self-consistent n_{DD} are shown, for different Γ in (**a**), and different U in (**b**). The energy unit in all figures is meV. In (**a**), $eV = U = 2.0$ meV. In (**b**), $eV = U$ and $\Gamma = 0.1$ meV. The scattered symbols are located by numerical data and the straight lines are plots of the function $I_M^{\downarrow} = k n_{DD} = k(1/2 - n_{2\uparrow})$ with different slopes. The k vs. $(\Gamma/U)^2$, and $I_M = I_M^{\downarrow}$ vs. $T^{3/2}$ are shown in (**c**) and (**d**) respectively. The symbols are from calculated data and the linear lines are fitting.
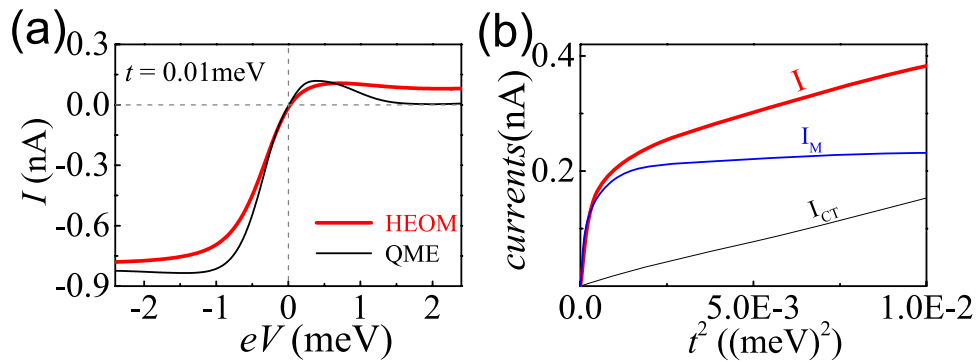
Figure 4. (**a**) The spin–degenerate counterparts to Fig. 2(a). (**b**) The spin–degenerate counterparts to Fig. 2(c).

Our theoretical results for titled QQDs further confirm the above arguments. In Fig. 5(c), I_{CT} is approximately proportional to t^6 at $E = U/3$. In Fig. 5(d), a similar peak structure is clearly seen with the resonant peak located at $E = U/3$, which is exactly the position of resonant doublons tunneling through four sites of tilted Hubbard chain, as observed in expriments[7]. We thus conclude that the MBT can support the coherent long-range tunneling of doublons in general systems, which is of both fundamental and practical importance. For example, the MBT can provide a feasible way to manipulate distant quantum gates or qubits in one step in solid-state quantum computing. This process would enhance the operating efficiency and fault-tolerant capability, compared to the nearest-neighbor control in exchange-based quantum gates[39].

Summary

In summary, we have theoretically discussed the many-body tunneling (MBT), by nonperturbatively solving the Anderson multi-impurity model, and identified it a fundamental tunneling process that involves the dynamics of doublons. Proportional to the numbers of dynamical doublons, the MBT is shown to dominate the off-resonant transport in strongly correlated systems. A $T^{3/2}$-dependence of the MBT current is uncovered and can be identified as a fingerprint of MBT in experiments. It is also proved that the MBT can support the coherent long-range tunneling of doublons. Our theoretical results are well consistent with recent experiments on the dynamics of
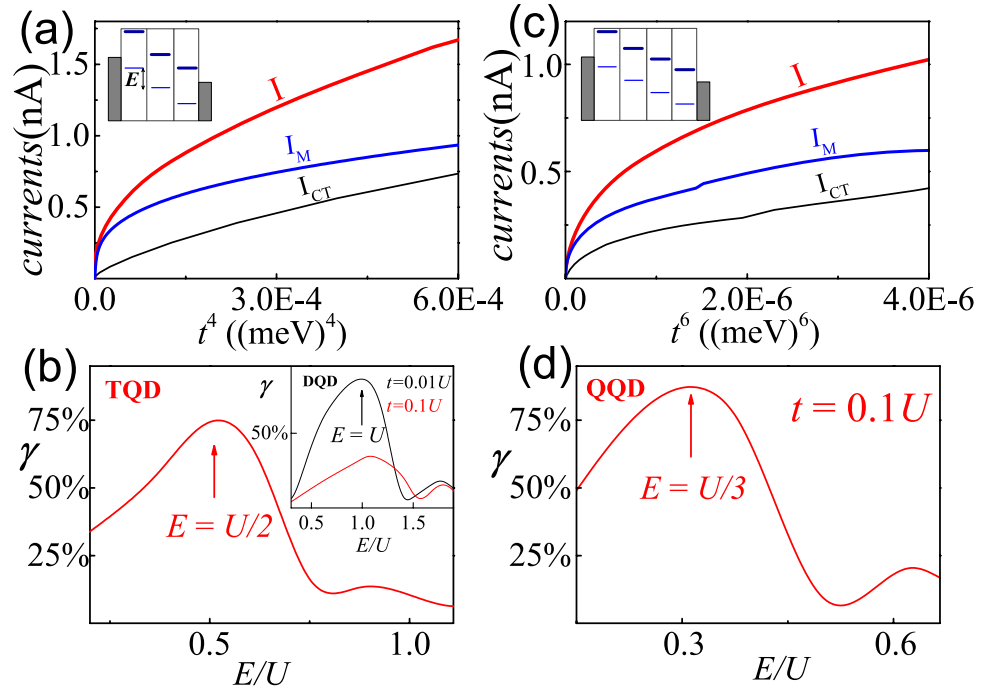
Figure 5. (**a**) The dependence of I, I_M and I_{CT} on t^4 at $eV = 1.5$ meV for the TQDs with tilting energy $E = U/2$. (**b**) The dependence of $\gamma \equiv (I_M/1) \times 100\%$ on the ratio of E/U in the TQDs at $t = 0.1U$ is displayed. The insert shows γ as a function of E/U in the DQDs at $t = 0.01U$ and $0.1U$. (**c**) The I, I_M and I_{CT} vary with t^6 at $eV = 1.5$ meV for the QQDs with $E = U/3$. (**d**) The γ as a function of E/U is depicted for the QQDs at $t = 0.1U$. The other parameters are $\epsilon_{i,s} = -U/2 = -1.0$ meV (TQD: $i = 1$–3; QQD: $i = 1$–4), $\Gamma = 0.1$ meV and $T = 0.1$ meV.

doublons. As a fundamental physical process, the MBT is expected to play important roles in more general systems beyond what we have discussed here.

Method

We take a serially coupled DQD system as an example to illustrate our method. It constitutes the open system of primary interest, and the surrounding reservoirs of itinerant electrons are treated as environment. The total Hamiltonian for the system is $H_T = H_S + H_B + H_{SB}$, where the interacting DQD

$$H_S = \sum_{i,s}\epsilon_{i,s}\hat{a}_{i,s}^\dagger\hat{a}_{i,s} + \frac{U}{2}\sum_{i,s}n_{i,s}n_{i\bar{s}} + t\sum_s(\hat{a}_{1,s}^\dagger\hat{a}_{2,s} + \text{H.c.}),$$ (2)

here $\hat{a}_{i,s}^\dagger$ ($\hat{a}_{i,s}$) is the operator that creates (annihilates) a spin-s electron with energy $\epsilon_{i,s}$ ($i = 1, 2$) in the dot i. $n_{i,s} = \hat{a}_{i,s}^\dagger\hat{a}_{i,s}$ corresponds to the operator for the electron number of dot i. U ($U = U_1 = U_2$) is the on-dot Coulomb interaction between electrons with spin s and $\bar{s}$ (opposite spin of s), while t is the interdot coupling strengths between the dot 1 and 2, determined by overlapping integral of them.

In what follows, the symbol μ is adopted to denote the electron orbital (including spin, space, etc.) in the system for brevity, i.e., $\mu = \{s, i \ldots\}$. The device leads are treated as noninteracting electron reservoirs and the Hamiltonian can be written as

$$H_B = \sum_{k\mu\alpha=L,R}\epsilon_{k\alpha}\hat{d}_{k\mu\alpha}^\dagger\hat{d}_{k\mu\alpha},$$ (3)

and the term of dot-electrode coupling is

$$H_{SB} = \sum_{k\mu\alpha}t_{k\mu\alpha}\hat{a}_\mu^\dagger\hat{d}_{k\mu\alpha} + \text{H.c.},$$ (4)

where $\epsilon_{k\alpha}$ is the energy of an electron with wave vector k in the α lead, and $\hat{d}_{k\mu\alpha}^\dagger$ ($\hat{d}_{k\mu\alpha}$) corresponds to the creation (annihilation) operator for an electron with the α-reservoir state $|k\rangle$ of energy $\epsilon_{k\alpha}$. To describe the stochastic nature of the transfer coupling, it can be written in the reservoir H_B-interaction picture as $H_{SB} = \sum_\mu\left[f_\mu^\dagger(t)\hat{a}_\mu + \hat{a}_\mu^\dagger f_\mu(t)\right]$, with $f_\mu^\dagger = e^{iH_Bt}\left[\sum_{k\alpha}t_{k\mu\alpha}^*\hat{d}_{k\mu\alpha}^\dagger\right]e^{-iH_Bt}$ being the stochastic interactional operator and satisfying the Gauss statistics. Here, $t_{k\mu\alpha}$ denotes the transfer coupling matrix element. The influence of electron reservoirs on the dots is taken into account through the hybridization functions, which is assumed Lorentzian

6

form, $\Delta_\alpha(\omega) \equiv \pi \sum_k t_{\alpha k \mu} t^*_{\alpha k \mu} \delta(\omega - \varepsilon_{k\alpha}) = \Delta W^2 / [2(\omega - \mu_\alpha)^2 + W^2]$, where Δ is the effective quantum dot-electrode coupling strength, W is the band width, and μ_α is the chemical potentials of the α ($\alpha = L, R$) lead.

In this paper, a hierarchical equations of motion approach (HEOM) developed in recent years is employed to study QD system[31, 32]. The HEOM based numerical approach is potentially useful for addressing the interacting strong correlation systems and has been employed to study dynamic properties, such as the dynamic Coulomb blockade Kondo, dynamic Kondo memory phenomena and time-dependent transport with Kondo resonance in QDs systems. The resulting hierarchical equations of motion formalism are in principle exact and applicable to arbitrary electronic systems, including Coulomb interactions, under the influence of arbitrary time-dependent applied bias voltage and external fields. The outstanding issue of characterizing both equilibrium and nonequilibrium properties of a general open quantum system are referred to in ref. 40. It is essential to adopt appropriate truncated level to close the coupled equations. The numerical results are considered to be quantitatively accurate with increasing truncated level and converge.

References

1. Kouwenhoven, L. P., Jauhar, S., Orenstein, J. & McEuen, P. L. Observation of Photon-Assisted Tunneling through a Quantum Dot. *Phys. Rev. Lett.* **73**, 3443 (1994).
2. Ambegaokar, V. & Baratoff, A. Tunneling Between Superconductors. *Phys. Rev. Lett.* **10**, 486 (1963).
3. Tanaka, Y. & Kashiwaya, S. Theory of Tunneling Spectroscopy of d-Wave Superconductors. *Phys. Rev. Lett.* **74**, 3451 (1995).
4. Friedman, J. R., Sarachik, M. P., Tejada, J. & Ziolo, R. Macroscopic Measurement of Resonant Magnetization Tunneling in High-Spin Molecules. *Phys. Rev. Lett.* **76**, 3830 (1996).
5. Hwang, H. Y., Cheong, S.-W., Ong, N. P. & Batlogg, B. Spin-Polarized Intergrain Tunneling in $La_{2/3}Sr_{2/3}MnO_3$. *Phys. Rev. Lett.* **77**, 2041 (1996).
6. Fölling, S., Trotzky, S., Cheinet, P., Feld, M., Saers, R., Widera, A., Müller, T. & Bloch, I. Direct observation of second-order atom tunneling. *Nature* **448**, 1029 (2007).
7. Meinert, F., Mark, M. J., Kirilov, E., Lauber, K., Weinmann, P., Gröbner, M., Daley, A. J. & Nägerl, H.-C. Observation of many-body dynamics in long-range tunneling after a quantum quench. *Science* **344**, 1259 (2014).
8. Grabert, H. & Devoret, M. H. *Single charge tunneling: Coulomb blockade phenomena in nanostructures*, NATO ASI Series Vol. 294 (Plenum Press, New York, 1992).
9. Nazarov, Y. V. & Blanter, Y. M. *Quantum transport: introduction to nanoscience*, Cambridge University Press, Cambridge, 2009).
10. Averin, D. V. & Nazarov, Yu. V. Virtual electron diffusion during quantum tunneling of the electric charge. *Phys. Rev. Lett.* **65**, 2446 (1990).
11. Hubbard, J. Electron correlations in narrow energy bands. *Proc. R. Soc. London, Ser. A* **276**, 283 (1963).
12. Kaplan, T. A., Horsch, P. & Fulde, P. Close Relation between Localized-Electron Magnetism and the Paramagnetic Wave Function of Completely Itinerant Electrons. *Phys. Rev. Lett.* **49**, 889 (1982).
13. Prelovšek, P., Kokalj, J., Lenarčič, Z. & McKenzie, R. H. Holon-doublon binding as the mechanism for the Mott transition. *Phys. Rev. B.* **92**, 235155 (2015).
14. Winkler, K., Thalhammer, G., Lang, F., Grimm, R., Hecker Denschlag, J., Daley, A. J., Kantian, A., Büchler, H. P. & Zoller, P. Repulsively bound atom pairs in an optical lattice. *Nature* **441**, 853 (2006).
15. Jördens, R., Strohmaier, N., Günter, K., Moritz, H. & Esslinger, T. A Mott insulator of fermionic atoms in an optical lattice. *Nature* **455**, 204 (2008).
16. Strohmaier, N., Greif, D., Jördens, R., Tarruell, L., Moritz, H., Esslinger, T., Sensarma, R., Pekker, D., Altman, E. & Demler, E. Observation of elastic doublon decay in the Fermi-Hubbard model. *Phys. Rev. Lett.* **104**, 080401 (2010).
17. Greif, D., Tarruell, L., Uehlinger, T., Jördens, R. & Esslinger, T. Probing nearest-neighbor correlations of ultracold fermions in an optical lattice. *Phys. Rev. Lett.* **106**, 145302 (2011).
18. Chudnovskiy, A. L., Gangardt, D. M. & Kamenev, A. Doublon relaxation in the Bose-Hubbard model. *Phys. Rev. Lett.* **108**, 085302 (2012).
19. Meinert, F., Mark, M. J., Kirilov, E., Lauber, K., Weinmann, P., Daley, A. J. & Nägerl, H.-C. Quantum quench in an atomic one-dimensional Ising chain. *Phys. Rev. Lett.* **111**, 053003 (2013).
20. Jürgensen, O., Meinert, F., Mark, M. J., Nägerl, H.-C. & Lühmann, D.-S. Observation of density-induced tunneling. *Phys. Rev. Lett.* **113**, 193003 (2014).
21. Xia, L., Zundel, L. A., Carrasquilla, J., Reinhard, A., Wilson, J. M., Rigol, M. & Weiss, D. S. Quantum distillation and confinement of vacancies in a doublon sea. *Nat. Phys* **11**, 316 (2015).
22. Covey, J. P., Moses, S. A., Gärttner, M., Safavi-Naini, A., Miecnikowski, M. T., Fu, Z., Schachenmayer, J., Julienne, P. S., Rey, A. M., Jin, D. S. & Ye, J. Doublon dynamics and polar molecule production in an optical lattice. *Nat. Commun.* **7**, 11279 (2016).
23. Anderson, P. W. Localized magnetic states in metals. *Phys. Rev* **124**, 41 (1961).
24. Ng, T. K. & Lee, P. A. On-site Coulomb repulsion and resonant tunneling. *Phys. Rev. Lett.* **61**, 1768 (1988).
25. Kondo, J. Resistance minimum in dilute magnetic alloys. *Prog. Theor. Phys.* **32**, 37C49 (1964).
26. Ono, K., Austing, D. G., Tokura, Y. & Tarucha, S. Current rectification by Pauli exclusion in a weakly coupled double quantum dot system. *Science* **297**, 1313 (2002).
27. Johnson, A. C., Petta, J. R., Marcus, C. M., Hanson, M. P. & Gossard, A. C. Singlet-triplet spin blockade and charge sensing in a few-electron double quantum dot. *Phys. Rev. B* **72**, 165308 (2005).
28. Liu, H. W., Fujisawa, T., Ono, Y., Inokawa, H., Fujiwara, A., Takashina, K. & Hirayama, Y. Pauli-spin-blockade transport through a silicon double quantum dot. *Phys. Rev. B* **77**, 073310 (2008).
29. Fransson, J. & Råsander, M. Pauli spin blockade in weakly coupled double quantum dots. *Phys. Rev. B* **73**, 205333 (2006).
30. Brunner, R., Shin, Y.-S., Obata, T., Pioro-Ladrière, M., Kubo, T., Yoshida, K., Taniyama, T., Tokura, Y. & Tarucha, S. Two-qubit gate of combined single-spin rotation and interdot spin exchange in a double quantum dot. *Phys. Rev. Lett.* **107**, 146801 (2011).
31. Li, Z. H., Tong, N. H., Zheng, X., Hou, D., Wei, J. H., Hu, J. & Yan, Y. J. Hierarchical Liouville-Space Approach for Accurate and Universal Characterization of Quantum Impurity Systems. *Phys. Rev. Lett.* **109**, 266403 (2012).
32. Jin, J. S., Zheng, X. & Yan, Y. J. Exact dynamics of dissipative electronic systems and quantum transport: Hierarchical equations of motion approach. *J. Chem. Phys.* **128**, 234703 (2008).
33. Hou, D., Wang, R., Zheng, X., Tong, N. H., Wei, J. H. & Yan, Y. J. Hierarchical equations of motion for an impurity solver in dynamical mean-field theory. *Phys. Rev. B* **90**, 045141 (2014).
34. Cheng, Y. X., Hou, W. J., Wang, Y. D., Li, Z. H., Wei, J. H. & Yan, Y. J. Time-dependent transport through quantum-impurity systems with Kondo resonance. *New J. Phys.* **17**, 033009 (2015).
35. Wei, J. H. & Yan, Y. J. Linear response theory for quantum open systems, *arXiv*:1108.5955 (2011).
36. Liu, H. W., Fujisawa, T., Hayashi, T. & Hirayama, Y. Pauli spin blockade in cotunneling transport through a double quantum dot. *Phys. Rev. B* **72**, 161305 (2005).

37. Wei, J. H., Xie, S. J., Mei, L. M., Berakdar, J. & Yan, Yi. Jing Conductance switching, hysteresis, and magnetoresistance in organic semiconductors. *Org. Electron.* **8**, 487 (2007).
38. Koppens, F. H. L., Folk, J. A., Elzerman, J. M., Hanson, R., Willems van Beveren, L. H., Vink, I. T., Tranitz, H. P., Wegscheider, W., Kouwenhoven, L. P. & Vandersypen, L. M. K. Control and detection of singlet-triplet mixing in a random nuclear field. *Science* **309**, 1346 (2005).
39. Loss, D. & DiVincenzo, D. P. Quantum computation with quantum dots. *Phys. Rev. A* **57**, 120 (1998).
40. Ye, L. Z., Wang, X. L., Hou, D., Xu, R. X., Zheng, X. & Yan, Y. J. HEOM-QUICK: a program for accurate, efficient, and universal characterization of strongly correlated quantum impurity systems, *WIREs Comp. Mol. Sci.* doi:10.1002/wcms.1269 (2016).

Acknowledgements

Author Contributions

W.J.H. and Y.D.W. performed the theoretical calculations. W.J.H., J.H.W., Z.G.Z. and Y.J. Yan analyzed the numerical data. W.J.H., J.H.W. and Z.G.Z. wrote the paper.

Additional Information

Competing Interests: The authors declare that they have no competing interests.

Publisher's note: Springer Nature remains neutral with regard to jurisdictional claims in published maps and institutional affiliations.